INTERNATIONAL JOURNAL FOR NUMERICAL METHODS IN FLUIDS
Int. J. Numer. Meth. Fluids 2008; **56**:209–232
Published online 30 May 2007 in Wiley InterScience (www.interscience.wiley.com). DOI: 10.1002/fld.1526

Numerical simulation of landslide impulsive waves by incompressible smoothed particle hydrodynamics

B. Ataie-Ashtiani*,† and G. Shobeyri‡

Department of Civil Engineering, Sharif University of Technology, Tehran, Iran

SUMMARY

An incompressible-smoothed particle hydrodynamics (I-SPH) formulation is presented to simulate impulsive waves generated by landslides. The governing equations, Navier–Stokes equations, are solved in a Lagrangian form using a two-step fractional method. Landslides in this paper are simulated by a submerged mass sliding along an inclined plane. During sliding, both rigid and deformable landslides mass are considered. The present numerical method is examined for a rigid wedge sliding into water along an inclined plane. In addition solitary wave generated by a heavy box falling inside water, known as Scott Russell wave generator, which is an example for simulating falling rock avalanche into artificial and natural reservoirs, is simulated and compared with experimental results. The numerical model is also validated for gravel mass sliding along an inclined plane. The sliding mass approximately behaves like a non-Newtonian fluid. A rheological model, implemented as a combination of the Bingham and the general Cross models, is utilized for simulation of the landslide behaviour. In order to match the experimental data with the computed wave profiles generated by deformable landslides, parameters of the rheological model are adjusted and the numerical model results effectively match the experimental results. The results prove the efficiency and applicability of the I-SPH method for simulation of these kinds of complex free surface problems. Copyright © 2007 John Wiley & Sons, Ltd.

Received 6 September 2006; Revised 9 April 2007; Accepted 15 April 2007

KEY WORDS: numerical method; impulsive wave; Tsunamis; landslide; Lagrangian method; incompressible SPH method

1. INTRODUCTION

Underwater landslides can generate surface water waves that have a high potential to cause damage and loss of life in coastal areas. Predicting the damage of these waves is of importance when assessing risk and magnitude of flooding in these areas.

*Correspondence to: B. Ataie-Ashtiani, Department of Civil Engineering, Sharif University of Technology, Tehran, Iran.
†E-mail: ataie@sharif.edu
‡Now Ph.D. student at Iran University of Science and Technology.

Due to the importance of waves generated by underwater landslides, researchers have accomplished many experimental studies of this phenomenon. Wiegel [1] generated water waves in constant depth channel by allowing rigid bodies to slide down a 22–54° inclined plane from the horizontal. Iwasaki [2] measured water wave heights resulting from horizontal motion of a sloping incline in a constant depth channel. Heinrich [3] conducted an underwater landslide experiment with a weighted block sliding down a 45° incline. Watts [4] described general features of water waves generated by under water landslides and scaled these features based on actual experimental results. Fritz *et al*. [5] investigated near-field characteristics of landslide generated impulsive waves in a two-dimensional physical laboratory model based on the generalized Froude similitude. Moreover, many numerical studies of landslide waves have been carried out by researchers. Jiang and LebLond [6] developed a fluid model to simulate water waves generated by deformable underwater landslides. Rzadkiewicz *et al*. [7] simulated an under water landslide by introducing a two-phase description of sediment motion and using the volume of fluid (VOF) technique. Grilli and Watts [8] simulated waves due to moving submerged body using a boundary element method.

A comprehensive review on the experimental and numerical studies about landslide waves have been provided by Ataie-Ashtiani and Najafi-Jilani [9, 10]. Moreover, Ataie-Ashtiani and Malek-Mohammadi studied the validity and accuracy of the existing empirical equations for predicting impulsive wave amplitude for the real cases [11].

Due to the complex motion of an underwater body of arbitrary geometry and interaction of waves with shoreline which results in non-linear governing equations, surface waves due to landslide are difficult to simulate. Recently, numerical models that do not use a grid have been used to overcome such difficulties. Moving-particle semi-implicit (MPS) is a mesh-less method in which each particle is followed in a Lagrangian manner leading to complete elimination of numerical diffusion problem that is usual in grids of Eulerian methods [12]. In MPS, the fluid is represented with particles. The motion of each particle is calculated through interactions with neighbouring particles by means of a kernel function. MPS has been successfully used to simulate a wide variety of problems such as dam breaks [13], solitary wave breaking on mild slopes [14] and vapour explosion [15]. The MPS model has been improved by Gotoh and Sakai [16] and later Gotoh *et al*. [17] applied the model for the wave generation due to large-scale landslides. In spite of the extensive applications of MPS method, still there are limitations for getting a stable solution. Ataie-Ashtiani and Farhadi [12] investigated the kernel functions for improving the stability of MPS method.

Smoothed particle hydrodynamics (SPH) is a mesh-less method introduced by Lucy [18] in astrophysics to study the collision of galaxies. Later Monaghan [19] extended the method and used it to deal with free surface problems. The SPH formulation is obtained as a result of interpolation between a set of disordered points known as particles. The interpolation is based on the theory of integral interpolants that uses a kernel function similar to a Gaussian which approximates a delta function. Each particle carries a mass, a velocity and all the properties of fluid with it.

Two different approaches have been used to extend SPH method to incompressible or nearly incompressible flows. In the first approach, real fluids are treated as compressible fluids with a sound speed which is much greater than the speed of bulk flow [19]. Pressure of particles in this method is computed by a stiff equation of state. This artificial compressibility can cause problems with sound wave reflection at boundaries and high sound speed leads to a stringent Courant–Friedrichs–Lewy (CFL) time step constraint [20, 21]. In the second approach, called incompressible-SPH (I-SPH) [14, 20, 21], unlike compressible SPH method, the pressure is directly obtained by solving a Poisson equation of pressure that satisfies incompressibility. The advantage of I-SPH lies in its ease and efficiency of free surface tracking using Lagrangian particles and the straightforward

DOI: 10.1002/fld

treatment of wall boundaries [20]. The first approach is known as SPH and the second one as I-SPH.

SPH and I-SPH have been used by many researchers to investigate different hydrodynamic problems such as the study of dam breaks [19, 21], gravity current descending a ramp [22], solitary wave breaking in mild slopes [14, 20], wave impact on tall structures [23], wave overtopping a deck [24], non-Newtonian flows with free surface [21] and incompressible separated flow [25]. For the impulsive and landslides water waves, SPH has also been used by De Girolamo *et al*. [26], Panizzo and Dalrymple [27], Panizzo *et al*. [28], Gallati and Braschi [29], Gallati *et al*. [30] and Monaghan *et al*. [31].

In this paper an I-SPH is introduced with the aim to enhance its stability and accuracy for free surface problems in comparison with the conventional I-SPH method. The objective of this work is to simulate waves generated by underwater landslide using I-SPH method and to show the efficiency and success of application of this method in simulation of these kinds of complex free surface problems. To the authors' knowledge, the I-SPH methods have not been used for the cases of the waves generated by landslides, especially when the landslide deformations are simulated simultaneously.

In Section 2 the governing equations are given and in Section 3 the I-SPH method and the imposed modifications on it are presented. Section 4 provides numerical examples and the comparison of numerical results with experimental and analytical results to examine the performance of the I-SPH.

2. GOVERNING EQUATIONS

The governing equations of viscous fluid flows that are mass and momentum conservation equations are presented in the following:

$$\frac{1}{\rho}\frac{\mathrm{D}\rho}{\mathrm{D}t} + \nabla.\mathbf{u} = 0 \tag{1}$$

$$\frac{\mathrm{D}\mathbf{u}}{\mathrm{D}t} = -\frac{1}{\rho}\nabla P + \mathbf{g} + \frac{\mu}{\rho}\nabla^2\mathbf{u} \tag{2}$$

where ρ [ML^{-3}] is the density, $\mathbf{u}$ [LT^{-1}] is the velocity vector, P [$\mathrm{ML}^{-1}\mathrm{T}^{-2}$] is the pressure and $\mathbf{g}$ [LT^{-2}] is the gravitational acceleration.

The computation of the I-SPH method is composed of two basic steps [20, 21]. The first step is the prediction step in which the velocity field is computed without including pressure gradient term in the momentum equation (Equation (2)):

$$\Delta\mathbf{u}_* = \left(\mathbf{g} + \frac{\mu}{\rho}\nabla^2\mathbf{u}\right)\Delta t \tag{3}$$

$$\mathbf{u}_* = \mathbf{u}_t + \Delta\mathbf{u}_* \tag{4}$$

$$\mathbf{r}_* = \mathbf{r}_t + \mathbf{u}_*\Delta t \tag{5}$$

where $\mathbf{u}_t$[LT^{-1}], $\mathbf{r}_t$[L] are the particle velocity and position at time t; $\mathbf{u}_*$[LT^{-1}], $\mathbf{r}_*$[L] are the temporary particle velocity and position, respectively; $\Delta\mathbf{u}_*$[LT^{-1}] is the change in the particle velocity during the prediction step.

DOI: 10.1002/fld

Incompressibility is not satisfied in this step and the fluid density ρ_* which is calculated based on the temporary particle positions deviates from the constant density (ρ_0).

In the second correction step, the pressure term is used to enforce incompressibility in the calculations:

$$\Delta \mathbf{u}_{**} = \frac{-1}{\rho_*} \nabla P_{t+1} \Delta t \tag{6}$$

$$\mathbf{u}_{t+1} = \mathbf{u}_* + \Delta \mathbf{u}_{**} \tag{7}$$

where $\Delta \mathbf{u}_{**}$ is the changed particle velocity during the correction step, P_{t+1} the particle pressure at time $t+1$ and $\mathbf{u}_{t+1}$ the velocity at time $t+1$.

By combining Equations (6) and (1) in order to set $\mathrm{D}\rho/\mathrm{D}t = 0$ at each particle according to the mass conservation equation after the prediction step, the Poisson equation is formulated as follows:

$$\nabla \cdot \left(\frac{1}{\rho_*} \nabla P_{t+1} \right) = \frac{\rho_0 - \rho_*}{\rho_0 \Delta t^2} \tag{8}$$

Finally, the new positions of particles are calculated by centred in time approximation:

$$\mathbf{r}_{t+1} = \mathbf{r}_t + \frac{\mathbf{u}_{t+1} + \mathbf{u}_t}{2} \Delta t \tag{9}$$

3. SPH FORMULATION

The key idea in this method, which is based on integral interpolant, is to consider that a function $A(r)$ can be approximated by [23]

$$A(\mathbf{r}_\mathrm{a}) = \sum_\mathrm{b} m_\mathrm{b} \frac{A_\mathrm{b}}{\rho_\mathrm{b}} W(|\mathbf{r}_\mathrm{a} - \mathbf{r}_\mathrm{b}|, h) \tag{10}$$

where a is the reference particle and b is its neighbouring particle. m_b [M] and $\rho_\mathrm{b}[\mathrm{ML}^{-3}]$ are mass and density, respectively, W is interpolation kernel, h [L] is the smoothing length which determines width of kernel and ultimately the resolution of the method. Thus, by summing over the particles the fluid density at particle a, $\rho_\mathrm{a}[\mathrm{ML}^{-3}]$, is evaluated according to Equation (10):

$$\rho_\mathrm{a} = \sum_\mathrm{b} m_\mathrm{b} W(|\mathbf{r}_\mathrm{a} - \mathbf{r}_\mathrm{b}|, h) \tag{11}$$

Kernel (weight) functions that directly affect the results of SPH method should have specific properties such as positivity, compact support, normalization, monotonically decreasing and delta function behaviour [23]. Many different kernel functions satisfying the required conditions have been proposed by researchers. The following kernel based on the spline function is widely used

DOI: 10.1002/fld

in the SPH formulation [32]:

$$\begin{aligned} W(r,h) &= \frac{10}{7\pi h^2}\left(1-\frac{3}{2}q^2+\frac{3}{4}q^3\right), \quad q\leqslant 1 \\ W(r,h) &= \frac{10}{28\pi h^2}(2-q)^3, \quad 1<q\leqslant 2 \\ W(r,h) &= 0, \quad q>2 \end{aligned} \tag{12}$$

where h [L] is the smoothing length, r [L] is distance between particles and $q=r/h$. In this paper this kernel function is used.

The gradient term in the Navier–Stokes (N–S) equation can have different forms in SPH formulation. Monaghan [32] proposed a model of gradient that conserves linear and angular momentum:

$$\left(\frac{1}{\rho}\nabla P\right)_{\mathrm{a}} = \sum_{\mathrm{b}} m_{\mathrm{b}}\left(\frac{P_{\mathrm{a}}}{\rho_{\mathrm{a}}^2}+\frac{P_{\mathrm{b}}}{\rho_{\mathrm{b}}^2}\right)\nabla_{\mathrm{a}} W \tag{13}$$

Laplacian will lead to the second derivative of the kernel function that is very sensitive to particle disorder and can cause pressure instability. Thus, developing a model of Laplacian that prevents this instability is very important. The following model of Laplacian has specific characteristic and is stable [20, 21]:

$$\nabla\cdot\left(\frac{1}{\rho}\nabla P\right)_{\mathrm{a}} = \sum_{\mathrm{b}} m_{\mathrm{b}}\frac{8}{(\rho_{\mathrm{a}}+\rho_{\mathrm{b}})^2}\frac{P_{\mathrm{ab}}\mathbf{r}_{\mathrm{ab}}.\nabla_{\mathrm{a}} W_{\mathrm{ab}}}{|\mathbf{r}_{\mathrm{ab}}|^2+\eta^2} \tag{14}$$

where $P_{\mathrm{ab}}[\mathrm{ML}^{-1}\,\mathrm{T}^{-2}] = P_{\mathrm{a}} - P_{\mathrm{b}}$, $\mathbf{r}_{\mathrm{ab}}[\mathrm{L}] = \mathbf{r}_{\mathrm{a}} - \mathbf{r}_{\mathrm{b}}$ and η [L] $= 0.1\,h$.

The corresponding coefficient matrix of the linear equations (Equation (14)) is scalar, symmetric and positive definite and can be efficiently solved by an iterative scheme.

By using the same approach, viscosity term is formulated as

$$\left(\frac{\mu}{\rho}\nabla^2\mathbf{u}\right)_{\mathrm{a}} = \sum_{\mathrm{b}}\frac{4m_{\mathrm{b}}(\mu_{\mathrm{a}}+\mu_{\mathrm{b}})\mathbf{r}_{\mathrm{ab}}.\nabla_{\mathrm{a}} W_{\mathrm{ab}}}{(\rho_{\mathrm{a}}+\rho_{\mathrm{b}})^2(|r_{\mathrm{ab}}|^2+\eta^2)}(\mathbf{u}_{\mathrm{a}}-\mathbf{u}_{\mathrm{b}}) \tag{15}$$

where μ [$\mathrm{ML}^{-1}\,\mathrm{T}^{-2}$] is the viscosity coefficient.

After employing the SPH formulation Equation (14) for the Laplacian operator, the corresponding coefficient matrix of linear equations is symmetric and positive definite and can be efficiently solved by available solvers.

In spite of the robustness of I-SPH in solving N–S equations with the incompressibility assumption, some errors are generated due to the discretization of the governing equations, the method of imposing boundary conditions and also the system of linear equations solvers. These errors prevent completely satisfying incompressibility conditions. Due to these errors, at each time step, a density error is generated and accumulated to the errors generated in the previous time steps.

If density of a single particle denoted with a at time $t=0$ is ρ_0, due to the above-mentioned errors the density of this particle at time t will be

$$\rho_0 = \rho_{\mathrm{a}}^t + \Delta\rho_{\mathrm{a}}^t \tag{16}$$

where ρ_{a}^t, $\Delta\rho^t$ are density of particle a and density error at time t. At the prediction step of time t, the temporary density of the particle is indicated as ρ_*. At the correction step after including

DOI: 10.1002/fld

the gradient pressure term in Equation (2)

$$\rho_{\mathrm{a}}^{t+1} = \rho_* + \Delta\rho_* \tag{17}$$

$$\rho_0 = \rho_{\mathrm{a}}^{t+1} + \Delta\rho_{\mathrm{a}}^{t+1} \tag{18}$$

By combining Equations (17) and (18)

$$\rho_0 = \rho_* + \Delta\rho_* + \Delta\rho_{\mathrm{a}}^{t+1} \tag{19}$$

where $\Delta\rho_*$ is the deviation of density due to not including pressure term in Equation (2) at the prediction step.

In I-SPH method, the source term of the Poisson equation (Equation (8)) for the particle is computed by

$$\frac{\rho_0 - \rho_*}{\rho_0 \Delta t^2} = \frac{\Delta\rho_* + \Delta\rho_{\mathrm{a}}^{t+1}}{\rho_0 \Delta t^2} \tag{20}$$

In the source term only $\Delta\rho_*$ should contribute, but in the I-SPH both parts of $\Delta\rho_*$ and $\Delta\rho_{\mathrm{a}}^{t+1}$ are considered. In our work a modification in this regard has been applied by including only $\Delta\rho_*$ in the source term. This means that the previous density errors are not allowed to affect the source term.

Changes in the fluid density can be computed through

$$\frac{\mathrm{d}\rho_{\mathrm{a}}}{\mathrm{d}t} = \sum_{\mathrm{b}} m_{\mathrm{b}} \frac{\mathrm{d}(W_{\mathrm{ab}})}{\mathrm{d}t} \tag{21}$$

and also changes in the values of the kernel function:

$$\frac{\mathrm{d}W(x_{\mathrm{ab}}, y_{\mathrm{ab}})}{\mathrm{d}t} = \left(\frac{\partial W_{\mathrm{ab}}}{\partial x} \frac{\mathrm{d}x_{\mathrm{ab}}}{\mathrm{d}t} + \frac{\partial W_{\mathrm{ab}}}{\partial y} \frac{\mathrm{d}y_{\mathrm{ab}}}{\mathrm{d}t} \right) = \nabla_{\mathrm{a}} W_{\mathrm{ab}} \mathbf{u}_{\mathrm{ab}} \tag{22}$$

where $\mathbf{u}$ is velocity and $\mathbf{u}_{\mathrm{ab}} = \mathbf{u}_{\mathrm{a}} - \mathbf{u}_{\mathrm{b}}$.

Change in the density of the particle at the prediction step is

$$\frac{\Delta\rho_*}{\rho_0 \Delta t^2} = \frac{1}{\rho_0 \, \mathrm{d}t} \frac{\mathrm{d}\rho}{\mathrm{d}t} \tag{23}$$

By combining Equations (21) and (23), the new source term is described with

$$\frac{1}{\rho_0 \, \mathrm{d}t} \sum_{\mathrm{b}} m_{\mathrm{b}} (\mathbf{u}_{\mathrm{a}} - \mathbf{u}_{\mathrm{b}}) \nabla_{\mathrm{a}} W_{\mathrm{ab}} \tag{24}$$

And finally the Poisson equation of pressure is described as

$$\nabla \cdot \left(\frac{1}{\rho_*} \nabla P_{t+1} \right) = \frac{1}{\rho_0 \, \mathrm{d}t} \sum_{\mathrm{b}} m_{\mathrm{b}} (\mathbf{u}_{\mathrm{a}} - \mathbf{u}_{\mathrm{b}}) \nabla_{\mathrm{a}} W_{\mathrm{ab}} \tag{25}$$

The same procedure can be used for all particles.

In this form of Poisson equation of pressure, the numerical density errors generated in the previous time steps do not affect the source term and stability and accuracy of I-SPH method are improved [33].

DOI: 10.1002/fld

3.1. Numerical treatment of free surfaces and wall boundaries

3.1.1. Solid walls. Solid walls are simulated by particles where the Poisson equation of pressure is solved. This balances the pressure of inner fluid particles and prevents them from accumulating in the vicinity of solid boundary. Also several lines of dummy particles are placed outside walls according to the initial configuration to keep the fluid particle density near walls consistent with inner fluid particles. The homogeneous Neumann boundary conditions are enforced when solving the equation of pressure [20]. In other words, the pressure of a dummy particle is set to that of a wall particle in the normal direction of the solid walls.

3.1.2. Free surface. Since there are no particles in the outer region of free surface, the particle density decreases on this boundary. A particle which satisfies the following equation is considered to be on the free surface, β being the free surface parameter:

$$\rho_* < \beta \rho_0 \tag{26}$$

where $0.8 < \beta < 0.99$ [13]. In this paper $\beta = 0.95$ and $h = 1.2 l_0$ are used, where l_0 is the initial particle spacing.

In the conventional I-SPH method, after recognizing the particles on the free surface, zero pressure is assigned to them. Since the particles density on free surface decrease discontinuously, spurious pressure gradients occurs if Equation (13) is used. To avoid this problem, special treatments should be considered when computing gradient operator for free surface particles. Let us assume that s is a surface particle with zero pressure and i is an inner fluid particle with pressure P_i. In order to calculate the pressure gradient between these two particles, a mirror particle, m, with pressure, P_i, should be placed in the direct reflection position of inner particle i through the surface particle s (Figure 1). In this way, the zero pressure condition on the free surface is satisfied [20].

The gradient of the pressure between the free surface particle s, mirror particle m and inner particle i is expressed as

$$\left(\frac{1}{\rho}\nabla P\right)_\mathrm{s} = m\left(\frac{P_\mathrm{s}}{\rho_\mathrm{s}^2} + \frac{P_\mathrm{i}}{\rho_\mathrm{i}^2}\right)\nabla_\mathrm{a} W + m\left(\frac{P_\mathrm{s}}{\rho_\mathrm{s}^2} + \frac{P_m}{\rho_m^2}\right)\nabla_\mathrm{a} W \tag{27}$$

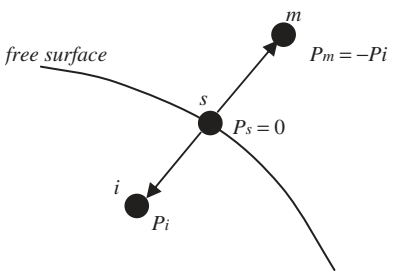

Figure 1. Free surface boundary treatment relationship between inner, mirror and free surface particle.

DOI: 10.1002/fld

$$P_{\mathrm{m}} = -P_{\mathrm{i}}$$

$$P_{\mathrm{s}} = 0 \tag{28}$$

$$\nabla_{\mathrm{s}} W_{\mathrm{sm}} = -\nabla_{\mathrm{s}} W_{\mathrm{si}}$$

Combining Equations (27) and (28) gives

$$\left(\frac{1}{\rho}\nabla P\right)_{\mathrm{s}} = 2m\left(\frac{P_{\mathrm{i}}}{\rho_{\mathrm{i}}^2}\right)\nabla_{\mathrm{a}} W \tag{29}$$

Therefore, the computed amount of gradient for free surface particles is double. In I-SPH method there is no control over incompressibility condition for the free surface particles as the Poisson pressure equation is not solved for these particles. Using Equation (14) for these particles leads to instability in computations. Regarding Equation (29), it is deduced that the Laplacian between free surface particle s and inner fluid particle i is expressed as

$$\nabla \cdot \left(\frac{1}{\rho}\nabla P\right)_{\mathrm{si}} = 2\left(m_{\mathrm{s}} \frac{8}{(\rho_{\mathrm{s}} + \rho_{\mathrm{i}})^2} \frac{P_{\mathrm{si}} \mathbf{r}_{\mathrm{si}} . \nabla_{\mathrm{s}} W_{\mathrm{si}}}{|\mathbf{r}_{\mathrm{si}}|^2 + \eta^2}\right) \tag{30}$$

By employing these modifications, satisfying directly incompressibility condition for free surface particles and the new form of source term of pressure Laplace equation, stability and accuracy of the present method are improved. The effects of these modifications have been tested for some problems such as dam break, evolution of a drop, breaking waves on mild slopes [33]. Here, the modified method has been called the present I-SPH.

4. TEST PROBLEMS

In this section three experimental cases are numerically simulated using the present numerical model. In Section 4.1, the experimental results of Heinrich [3] for landslides waves generated by rigid bodies (landslides) are used to compare with those of I-SPH. In Section 4.2, solitary waves due to a heavy box falling into water, known as Scott Russell wave generator, are computationally simulated and results are compared with the experimental data of Monaghan and Kos [34]. In Section 4.3 the deformation of landslides is simulated and the landslide behaviour is considered as non-Newtonian fluids [7].

4.1. Underwater rigid landslide

In this section, the present numerical model is used for simulating waves generated by a rigid wedge sliding into water along an inclined plane which is a laboratory experiment performed by Heinrich [3]. In this experiment water waves were generated by allowing a wedge to freely slide down a plane inclined 45° on the horizontal. The wedge was triangular in cross section (0.5 m × 0.5 m) and with a density of 2000 kg/m^3. Water depth was 1m and the top of the wedge was initially 1 cm below the horizontal free surface. The computational domain shown in Figure 2 was 4 m by 1.3 m in the x and y directions. A constant time step ($\Delta t = 0.001$ s) and initial particle spacing ($l_0 = 0.04$ m) were used in the computations.

DOI: 10.1002/fld

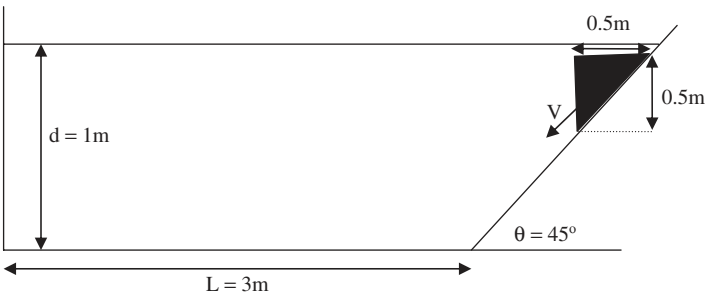

Figure 2. Initial conditions of the rigid wedge sliding down a plane inclined 45° on the horizontal.

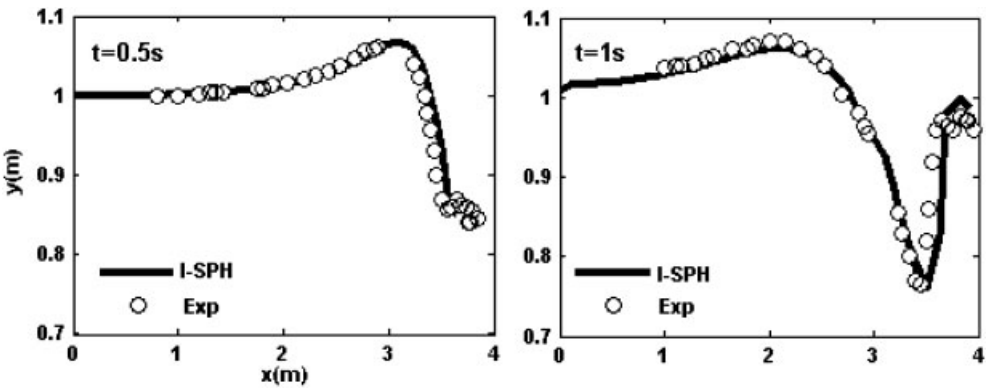

Figure 3. Comparison between I-SPH (continuous line) and experimental (circle) water surface elevations at $t = 0.5$ and 1 s for the rigid wedge sliding down a plane inclined 45° on the horizontal.

After an acceleration phase lasting about 0.4 s, the box reached a terminal velocity of 0.6 m/s. The vertical velocity of the wedge during the acceleration phase can be described by [8]

$$\begin{aligned} u(t) &= c_1 \tanh(c_2 t), \quad t \leqslant 0.4\,\text{s} \\ u(t) &= 0.6, \quad t > 0.4\,\text{s} \end{aligned} \tag{31}$$

c_1 and c_2 are constant values that in our computations were 86 and 0.0175, respectively.

At each time step the velocity of the wedge is known and based on that the position of the wedge is determined. The same procedure is also used for test Problem 4.2.

Comparison between the experimental and the simulated wave profiles at $t = 0.5$ and 1 s is shown in Figure 3. The good agreement between experimental data [7] and computational results proves the ability of the present method to successfully simulate such flows. The maximum height of the water above the still water level at $t = 0.8$ s is about 7 cm.

Particle configuration due to sliding of the rigid wedge is presented at different times until $t = 3$ s in Figure 4, showing the stability of the present method to simulate the problems for long times. There is no experimental data [7] for $t > 1$ s. The generated wave moves towards the left wall and at about $t = 1.5$ s the wave reflects from the wall and at about $t = 3$ s the water surface

DOI: 10.1002/fld

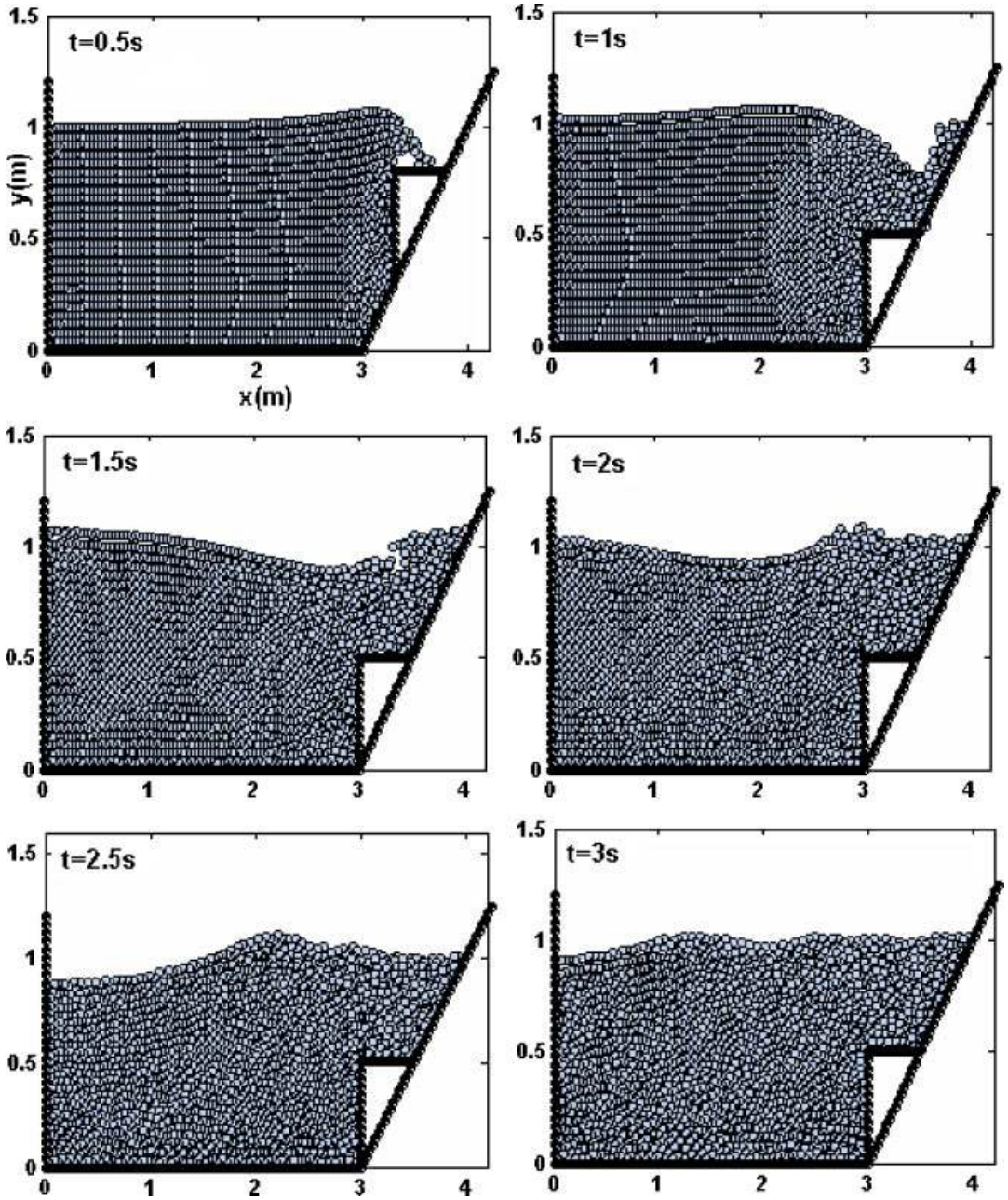

Figure 4. I-SPH particles configuration for the rigid wedge sliding down a plane inclined 45° on the horizontal at different times.

DOI: 10.1002/fld

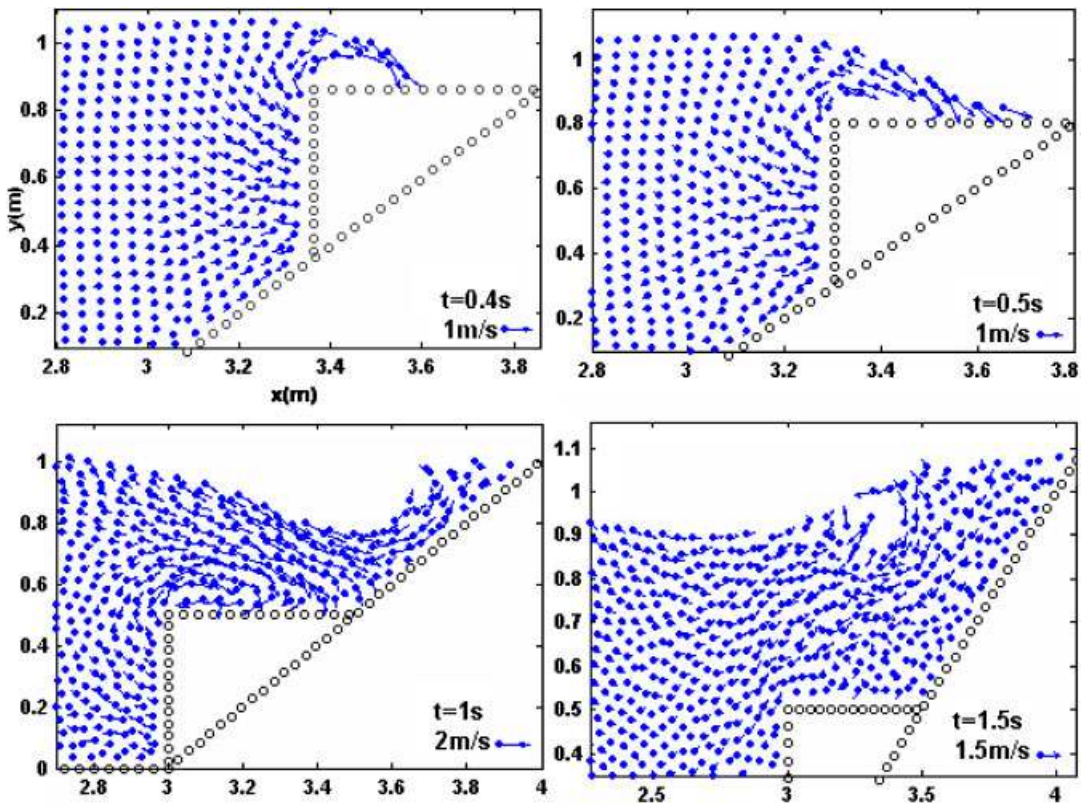

Figure 5. Velocity field for the rigid wedge sliding down a plane inclined 45° on the horizontal at different times computed by the present method.

is nearly horizontal. The elevation of water at $t = 1.5$ s near the left wall is about 106.6 cm. In Figure 5 the velocity field of the problem is presented at different times. At $t = 1$ s a vortex is being generated above the wedge and at $t = 1.5$ s the water is changing its direction and the intensity of velocity field is decreased after the wedge has reached the bottom, as expected. As shown in Figure 6, the pressure field computed for different times by the I-SPH method indicates that, due to the occurrence of zero velocity of particles far from the box, the pressure of these particles is nearly hydrostatic. In Figure 7 the water surface elevation for two fixed points located at $x = 1$ and 2 m measured from the left wall is recorded. The maximum elevation of the first point ($x = 2$ m, $t \approx 1$ s) is about 107.4 cm and for the second point ($x = 1$ m, $t \approx 1.3$ s) is about 106.8 cm. Both maximum surface elevations are close to the maximum water elevation derived from experimental data [7] at $t = 1$ s and $x \approx 2$ m, showing the accuracy of the present method.

4.2. Scott Russell wave generator

In the previous section, the wave generated due to sliding of a submerged wedge was analysed. In this section, solitary waves generated by a heavy box falling vertically into water are considered. Monaghan and Kos [34] examined this problem both experimentally and numerically (using the

DOI: 10.1002/fld

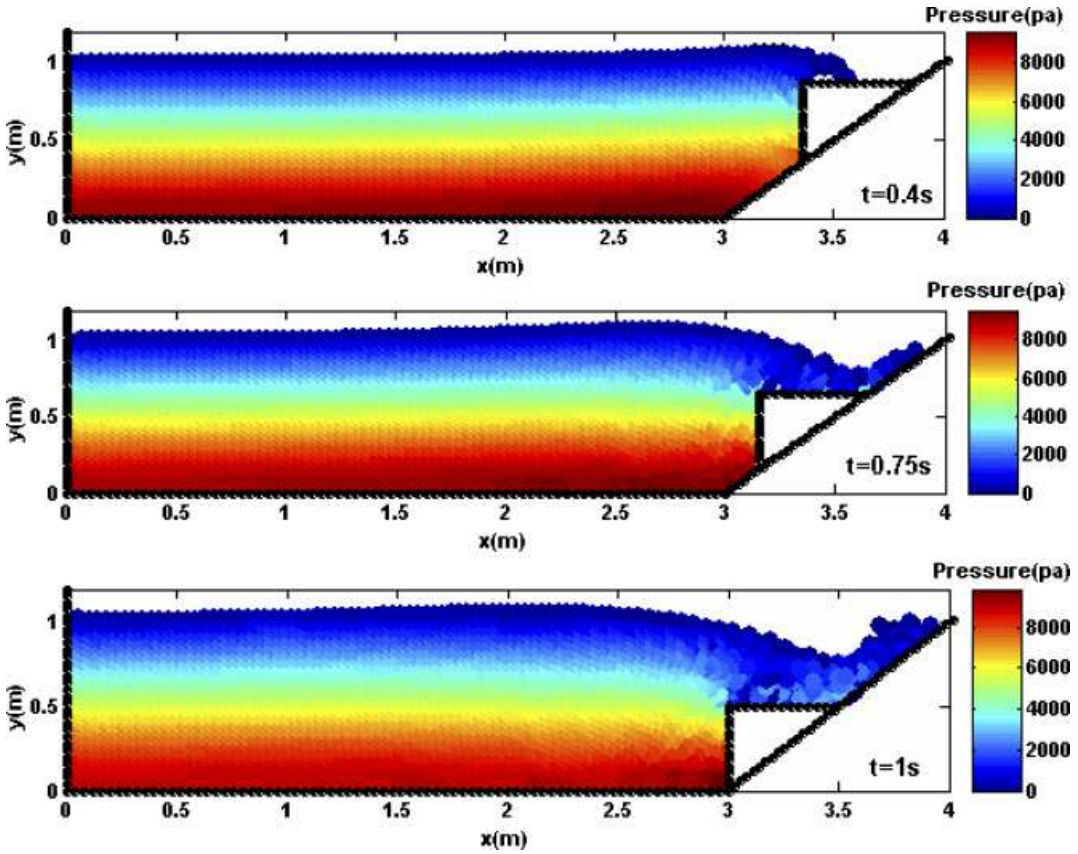

Figure 6. Pressure field for the rigid wedge sliding down a plane inclined 45° on the horizontal at different times computed by the present method.

SPH method). The experiment involved a weighted box dropping vertically into a wave tank. The box was 0.3 m × 0.4 m. Three different water depths were considered in the experiment but in this paper we will only consider the case with water depth equal to 0.21 m. The initial condition of the problem is shown in Figure 8. It should be noted that the horizontal length of the numerical tank is assumed to be 2 m, much shorter than the experimental tank (9 m). However, we believe that the difference in the length of tanks does not influence the results. To prevent splash, the bottom of the box was initially placed 0.5 cm below the water surface in the experiment [34]. The vertical velocity of the box is expressed by [34]

$$\frac{V}{\sqrt{gD}} = 1.03\frac{Y}{D}\left(1 - \frac{Y}{D}\right)^{0.5} \tag{32}$$

where D is the depth of the water, Y the height of the bottom of the box above the bottom of the tank at time t, g the acceleration of gravity and V the falling vertical velocity of the box at time t. Time step in this case is controlled with Courant number ($\Delta t < 0.1 l_0 / V_{\max}$) where $V_{\max}$ is maximum velocity of particles at each time step [21].

DOI: 10.1002/fld

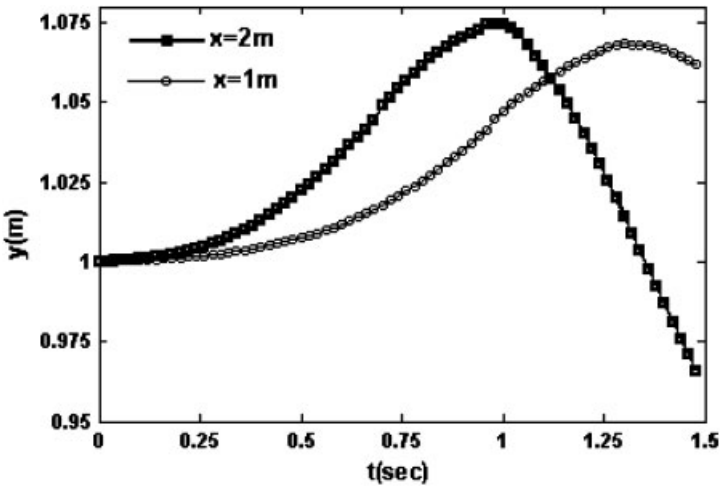

Figure 7. I-SPH water surface elevations at 1 m (circles) and 2 m (black squares) from the left end of the tank at different times.

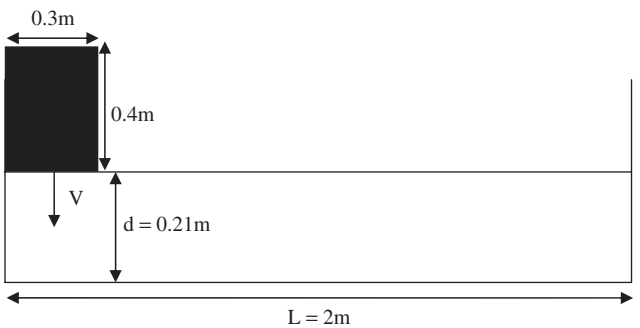

Figure 8. Initial conditions of Scott Russell wave generator test case.

The profile of the solitary wave generated by the falling box into the water can be expressed by [20]

$$H(x,t) = a\,\mathrm{sech}^2\left[\sqrt{\frac{3a}{4d^3}}(x-ct)\right] \tag{33}$$

where H is the water surface elevation, a is the wave amplitude, d is the water depth and $c=\sqrt{g(d+a)}$ is the solitary wave celerity.

The horizontal velocity underneath the wave profile is given by [20]

$$u = H\sqrt{\frac{g}{d}} \tag{34}$$

DOI: 10.1002/fld

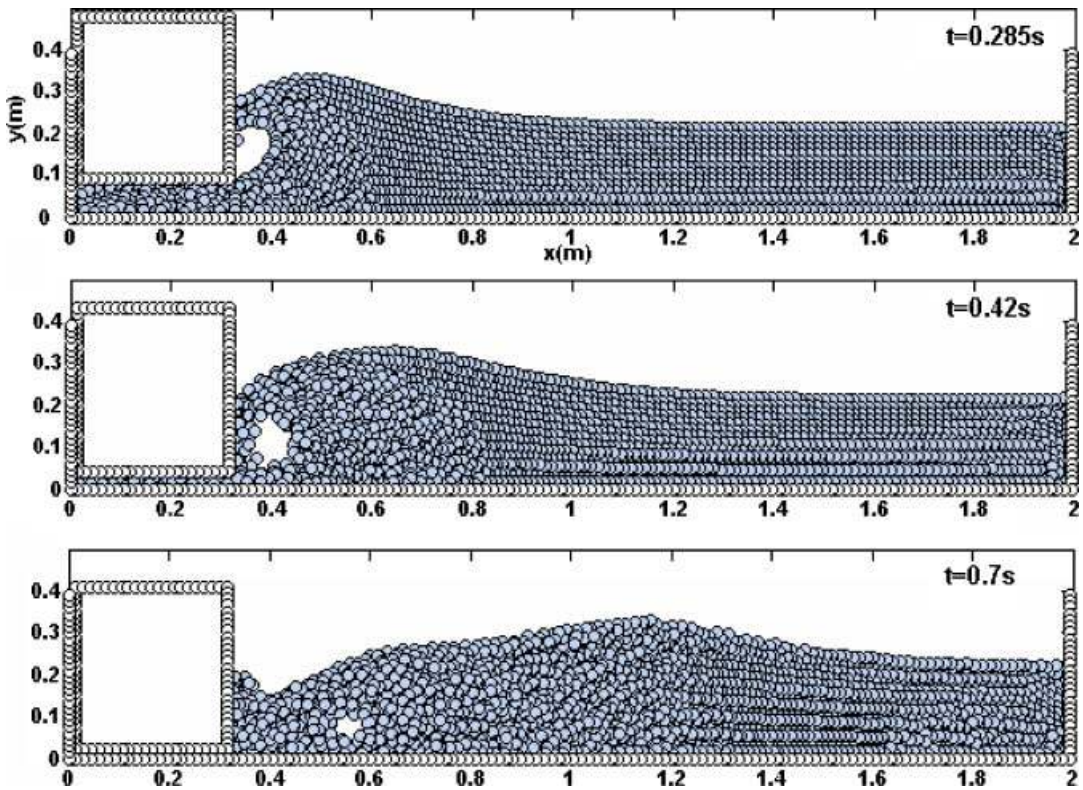

Figure 9. Particle configurations computed by the present method at different times for Scott Russell wave generator problem ($l_0 = 0.015$ m).

In Figure 9 particle configuration simulated by the present method shows the formation of a solitary wave and a plunging wave following the solitary wave down the tank. At $t = 0.7$ s the vortex is about approximately 23 cm far from the right box wall.

In Figure 10 the solitary wave generated by the falling box is shown and the profile of the wave is compared with Equation (33). The agreement between the analytical profile of the wave and the simulated free surface is good. It should be noted that the term '*x-ct*' in this equation is set so that the crest of the analytical corresponds to the crest of the numerically simulated wave and also the wave amplitude a (Equation (33)) is assumed to be 11 cm computed by the present method (using initial particle spacing $l_0 = 0.015$ m). Monaghan and Kos [34] solved the problem by SPH method. In their computation the computed amplitude was 10.8 cm (using $l_0 = 0.00525$ m) which is very close to the value gained in this paper. The experimental result for the wave amplitude is about 10 cm. These results show that in spite of much fewer particles used in the computations, the present method can simulate the problem properly.

In Figure 11 the horizontal velocity of free surface particles is compared with the analytical solution (Equation (34)) that once again demonstrates the accuracy of the model. Figure 12 shows some characteristic lengths, measured at $t = 0.285$ s [34] associated with the reverse plunging wave. The computed values of these parameters, for the present method and SPH method [34],

DOI: 10.1002/fld

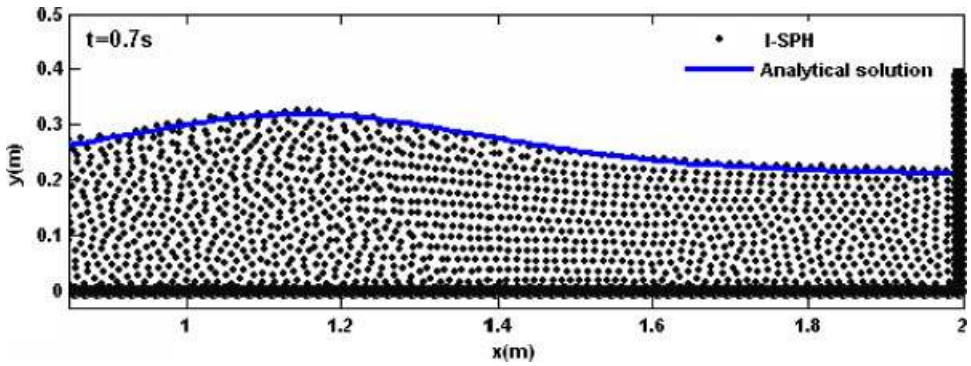

Figure 10. Comparison between computed wave profile by the present method and solitary wave analytical solution for Scott Russell wave generator problem at $t = 0.7$ s ($l_0 = 0.015$ m).

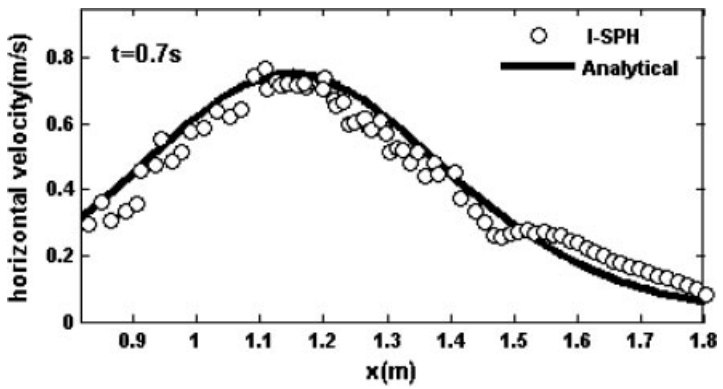

Figure 11. Comparison between the horizontal velocities of free surface particles computed by the present method and analytical solution of Scott Russell wave generator problem at $t = 0.7$ s ($l_0 = 0.015$ m).

are given in Table I. It should be considered that two different particles spacing have been used and for the present I-SPH, the number of particle is almost eight times less than that used in simulations presented in Monaghan and Kos [34]. In spite of the fewer particles employed in the present model, the computed value of these characteristic lengths are the same as those gained by SPH method. In the experiment parameter Y at $t = 0.285$ s was about 0.094 m, while in our computation using Equation (32) Y was about 0.088 m. To evaluate the goodness and accuracy of I-SPH simulations, we refer to parameter h rather than R (see Figure 12).

In Figure 13 the computed pressure field of this problem for different times is presented. At $t = 0.05$ s the maximum pressure is on the left corner of the tank and is about 4000 Pa showing significant deviation from hydrostatic pressure and under the box the maximum pressure is about 3400 Pa. Obviously, it is due to the dynamic pressure caused by the impact of box. At $t = 0.1625$ s the maximum pressure is about 4270 Pa and under the box the maximum pressure is 3200 Pa. At this time the pressure of the particles located between the box and the tank is approximately uniform. At $t = 0.285$ s the high-pressure region has moved and is about at $x = 0.6$ m with pressure of 2700 Pa

DOI: 10.1002/fld

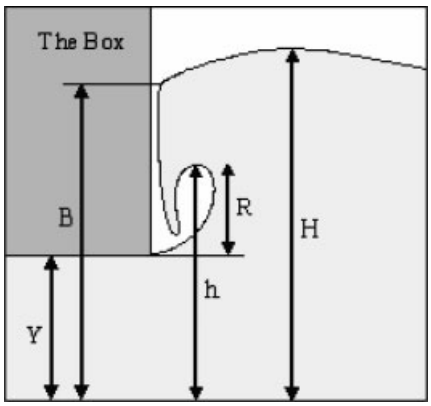

Figure 12. Definitions of the parameters of Scott Russell wave generator problem [34].

Table I. Comparison between the length h, H, B, R computed by the present method, SPH [34] and experimental results.

Initial particle spacing l_0 (m)	Method	H (m)	R (m)	h (m)	B (m)
0.015	I-SPH	0.329	0.13	0.218	0.255
0.01	I-SPH	0.3301	0.146	0.234	0.268
0.0105	SPH	0.308	0.075	0.169	0.273
0.007	SPH	0.308	0.099	0.193	0.261
0.00525	SPH	0.309	0.109	0.203	0.273
0.0042	SPH	0.3086	0.114	0.208	0.272
—	Experimental	0.333±0.01	0.1333±0.02	0.2273±0.02	0.303±0.02

and the maximum pressure under the box is about 890 Pa. Although the dynamic pressures under the box are still greater than those of the high-pressure region (around $x = 0.6$ m) but since the hydrostatic pressures at this region are much greater than those under the box therefore the total pressures around $x = 0.6$ m are greater. Far from the box, due to the disappearance of dynamic pressure, pressure is hydrostatic. In Figure 14 velocity field for the problem at $t = 0.285$ s is shown. As shown, particles around $x = 0.3$ m have a high velocity and the particles on the free surface have negligible velocity.

4.3. Deformable landslides

Section 4.1 showed results of the simulation of the water surface elevation due to the motion of a rigid body along an inclined surface. However, in real phenomena, deformation of a sliding mass cannot be neglected. In the next sub-sections the deformation of a sliding mass is simulated using a rheological model.

4.3.1. Rheological model. Following the approach of [7], it is here assumed that the sliding mass which represents the landslide behaves as a non-Newtonian fluid. There are many rheological

DOI: 10.1002/fld

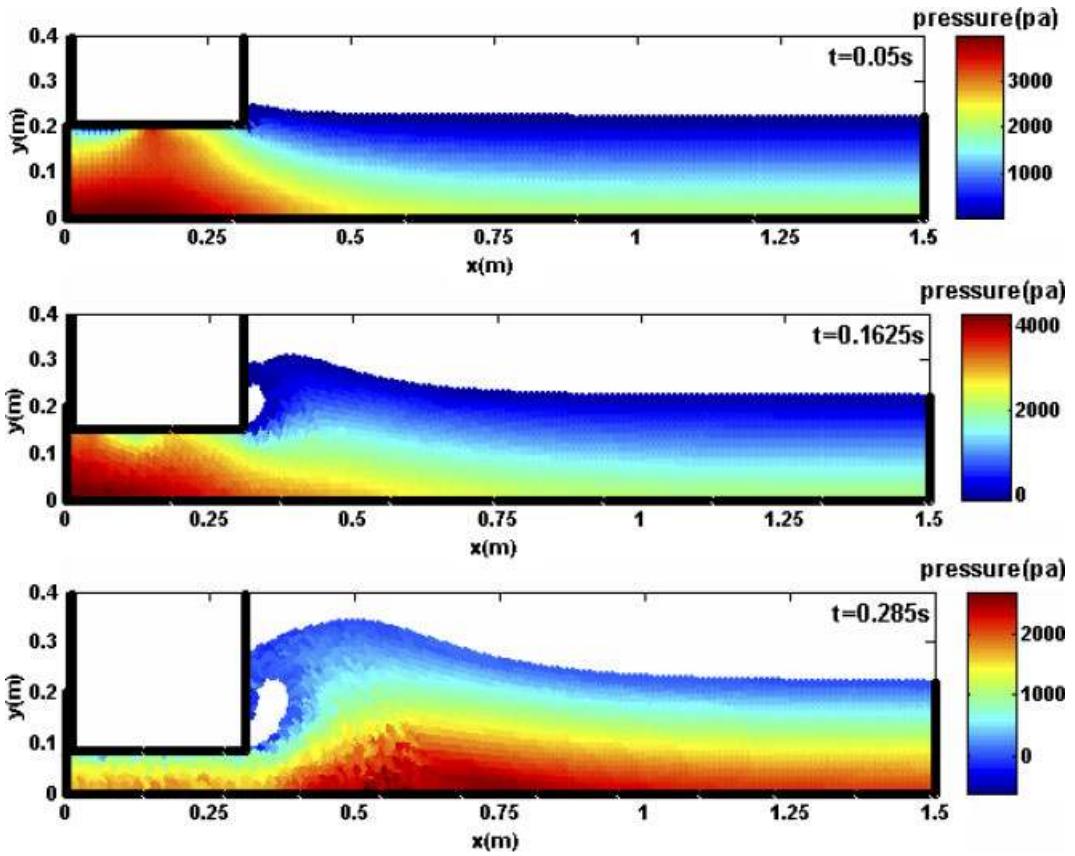

Figure 13. Pressure field computed by the present method at different times for Scott Russell wave generator problem ($l_0 = 0.01$ m).

models to simulate these fluids. The Bingham model is the simplest and the most known and it is expressed as [21]

$$\mu_{\text{eff}} = \mu_{\text{B}} + \frac{\tau_{\text{B}}}{\dot{\gamma}} \tag{35}$$

where μ_{B}, τ_{B} and $\dot{\gamma}$ are viscosity, Bingham yield stress and shear rate, respectively. In two dimensions, the shear rate $\dot{\gamma}$ simplifies to

$$\dot{\gamma} = \sqrt{2\left(\frac{\partial u}{\partial x}\right)^2 + 2\left(\frac{\partial v}{\partial y}\right)^2 + \left(\frac{\partial u}{\partial y} + \frac{\partial v}{\partial x}\right)^2} \tag{36}$$

where u and v are the components of the velocity vector.

In this model, the fluid behaves like a rigid body at shear rates below the yield stress, while it behaves like a Newtonian fluid at shear rates greater than the yield stress [21]. The general Cross

DOI: 10.1002/fld

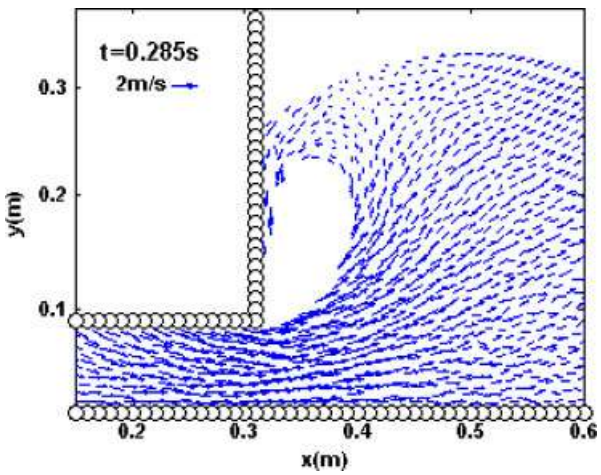

Figure 14. Velocity filed computed by the present method for Scott Russell wave generator problem at $t = 0.285$ s ($l_0 = 0.01$ m).

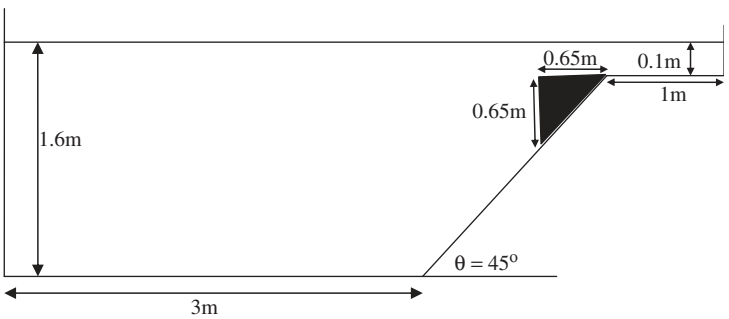

Figure 15. Initial conditions of the deformable landslide test case.

model is another rheological model that effectively simulates non-Newtonian fluids [35]:

$$\frac{\mu_0 - \mu_{\text{eff}}}{\mu_{\text{eff}} - \mu_\infty} = (K\dot{\gamma})^m \tag{37}$$

where μ_0, μ_∞ are viscosity at very low and very high shear rates, respectively; K and m are constant parameters. It should be noted that $\mu_\infty = \mu_B$ [21].

By combining Equations (35) and (37) and taking m as unity, the effective viscosity in the Cross model is defined as

$$\mu_{\text{eff}} = \frac{\mu_0 + \dfrac{\mu_0 \mu_\infty}{\tau_B}\dot{\gamma}}{1 + \dfrac{\mu_0}{\tau_B}\dot{\gamma}} \tag{38}$$

DOI: 10.1002/fld

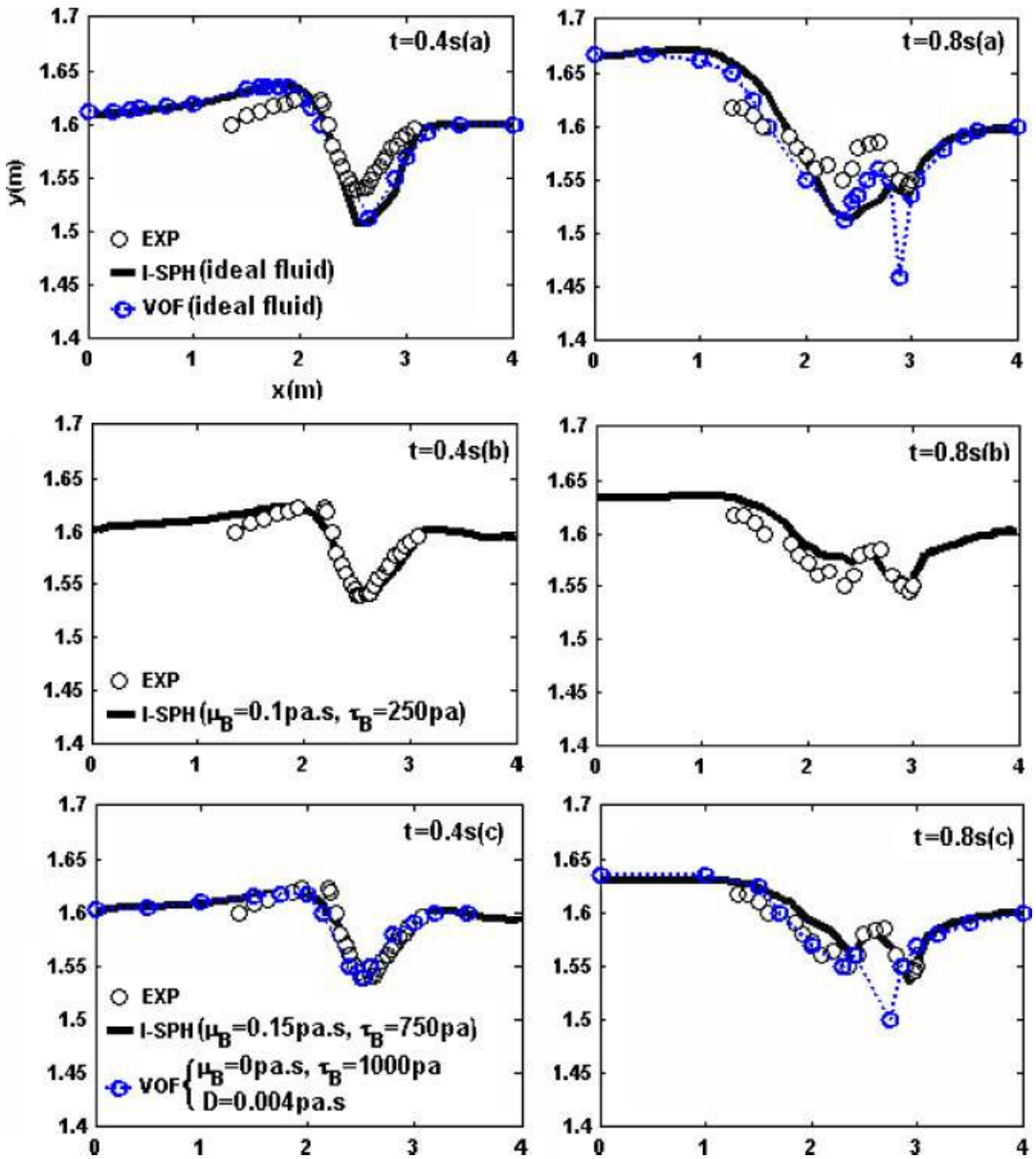

Figure 16. Comparison between computed (the present method, VOF [7]) and experimental wave profile for different cases of parameters of the rheology model for the deformable landslide problem at $t = 0.4$ and 0.8 s.

In order to avoid numerical instability, μ_0 is frozen at a fixed high value ($1000\mu_\infty$) [21]. It should be noted that under this condition, the Cross model, unlike the Bingham model, is a continuous variable.

DOI: 10.1002/fld

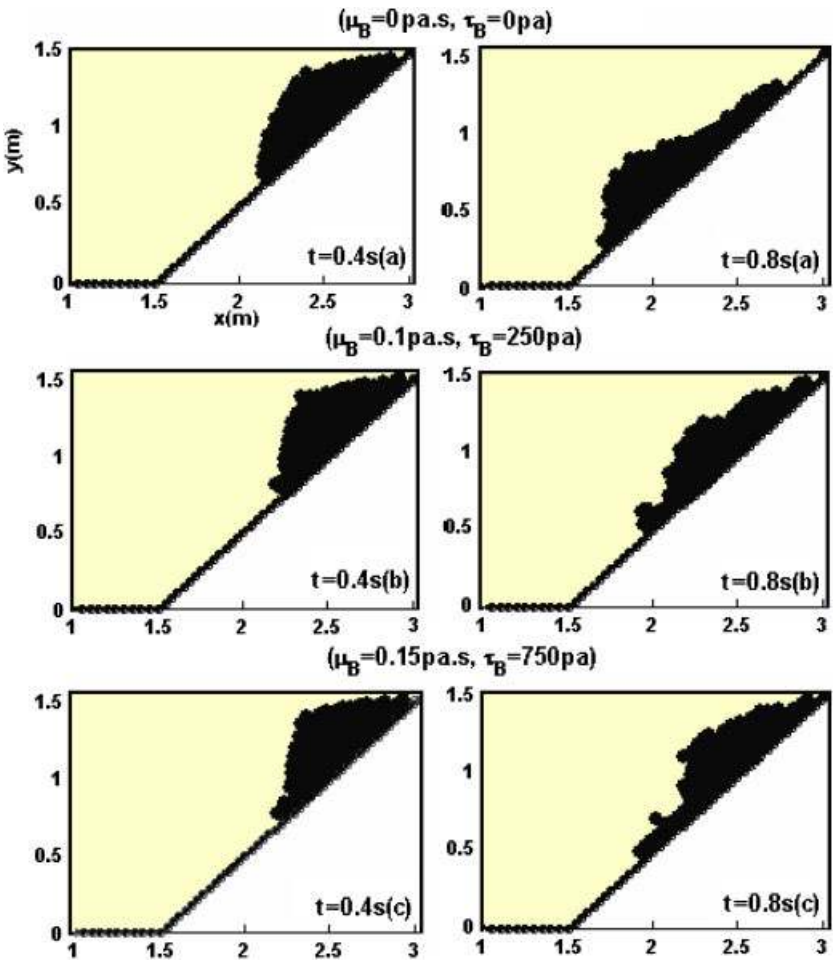

Figure 17. The shape of the sliding mass for different cases of parameters of the rheology model for the deformable landslide problem at $t = 0.4$ and 0.8 s computed by the present method.

4.3.2. Sand flows and associated water waves. A deformable landslide is simulated in the experiment carried out at CEMAGREF institute [7]. In the experiment a mass of sand with a mean density of 1950 kg/m^3 slides down an inclined plane with a slope of 45° on the horizontal. The initial condition of the problem is shown in Figure 15. An initial particle spacing equal to $l_0 = 0.05$ m and a constant time step $\Delta t = 0.005$ s are used in the computations.

In the first simulation, the sliding mass is modelled as an ideal fluid without rheological law. This means that in Equation (2) the viscosity term is not considered. Rzadkiewicz *et al.* [7] used the VOF method to solve the problem under this condition. As it can be seen in Figure 16(a), the agreement between the wave profiles at $t = 0.4$ and 0.8 s computed by the present method and the VOF is good but results of both methods do not match with the experimental data indicating that it is not correct to assume that the sliding mass behaves like an ideal fluid.

DOI: 10.1002/fld

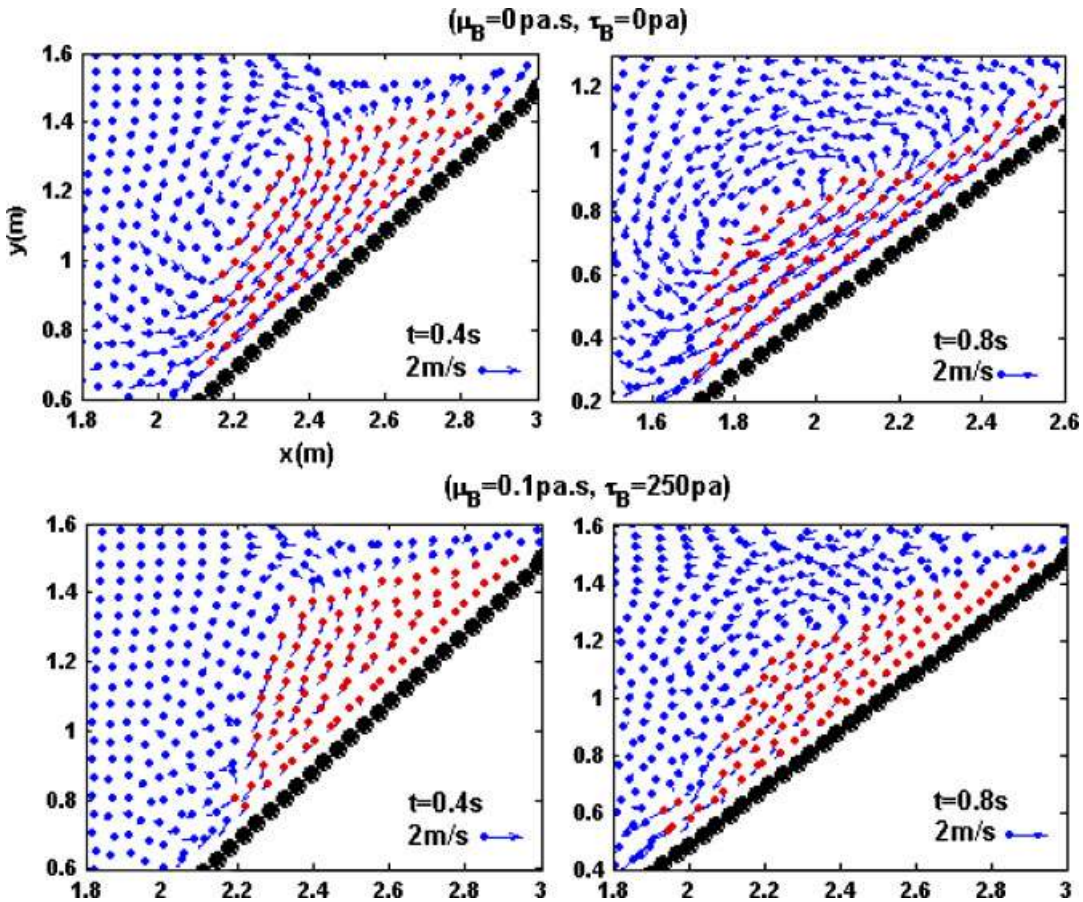

Figure 18. Velocity fields for the deformable landslide problem at $t = 0.4$ and 0.8 s for two cases of the rheology model computed by the present method.

In the absence of measurement of viscosity, the set of parameters used in the Cross model is adjusted by trial and error. In the second simulation, μ_B and τ_B are assumed to be 0.1 Pa s and 250 Pa, respectively. For this case, the VOF results have not been presented in [7]. The water surface elevation computed for this condition is shown in Figure 16(b). It is visible that the agreement between the computed and experimental wave profiles is satisfactory but in order to match the result better, a third simulation has been carried out by assuming $\mu_B = 0.15$ Pa s and $\tau_B = 750$ Pa. As illustrated in Figure 16(c), the larger value of yield stress (τ_B) and viscosity (μ_B) generate smaller waves which closely match the experimental results. This problem was solved by Rzadkiewicz *et al*. [7] with setting the parameters of the Bingham model ($\tau_B = 1000$ Pa, $\mu_B = 0$ Pa s, $D^{\S} = 0.004$ Pa s). The computational results of simulating this problem using the VOF method are shown in Figure 16(c). By comparing the computational results using the VOF [7]

[§] Diffusion coefficient.

DOI: 10.1002/fld

and the present I-SPH method with the experimental data, the capability of the present method to simulate complex problems efficiently and accurately is visible.

The shape of the sliding mass at $t = 0.4$ and 0.8 s for three simulations are shown in Figure 17. Figure 17(a) (real fluid) for $t = 0.8$ s shows that most of the mass is concentrated at the mud front but in the experiment [7] most of the sliding mass remains near the initial position. In the second simulation ($\mu_B = 0.1$ Pa s, $\tau_B = 250$ Pa) with including the Cross model parameters, the mass keeps its initial shape at $t = 0.4$ s (Figure 17(b)) and $t = 0.8$ s most of the mass remains close to the initial position. The same conclusion can be observed in Figure 17(c) for the third simulation. As at the beginning of the slide motion, velocity and shear rate (see Equations (36) and (38)) are small and it means that μ_{eff} is approximately similar for the second and third simulations. Therefore, shapes of the mass at $t = 0.4$ s are about the same (Figure 17(b) and (c)). The same conclusion can also be inferred for the water wave surface (see Figure 16(b) and (c)). A vortex moving along the slope during sliding of the mass at $t = 0.4$ and 0.8 s for the first and second simulation can be seen in Figure 18. For the first simulation the vortex is strong compared with the vortex of the second simulation. This is because of large viscosity in the second simulation leads to lower velocity.

It should be noticed that the numerical simulations were carried out considering no friction at the interface between ambient water and the mass.

5. CONCLUSION

In this paper the application of an incompressible SPH (I-SPH) method for numerical simulation of submarine landslide generated waves is presented. SPH is a mesh-less method in which particles are used to simulate the fluid. The method has the advantage of solving the governing equations by a Lagrangian approach. By employing a new form of source term to the Poisson equation of pressure and enforcing incompressibility to free surface particles, stability and accuracy of this method are improved.

The present I-SPH method is used to simulate a submerged rigid wedge sliding along an inclined surface. Also solitary waves generated by a heavy box falling into water, which is a good example for simulating falling avalanche in dam reservoirs and the behaviour of waves due to landslides near slopes are efficiently examined by the present method. The computational I-SPH results were in good agreement with the experimental data.

Then, the present model is used to simulate flow of gravel mass sliding along an inclined plane. Gravel mass is modelled as a non-Newtonian fluid. Comparison between the computed and experimental wave profiles generated by both the sliding rigid box and the deformable landslide shows the ability of the present method to successfully simulate such kind of complex problems.

NOMENCLATURE

c	solitary wave celerity
d	water depth
h	Kernel smoothing length
K	constant parameter in Cross model
l_0	initial particle spacing
m	particle mass

DOI: 10.1002/fld

P	pressure
$q = r/h$	non-dimensional distance between particles
r	distance between particles
$\mathbf{r}$	Position vector
$\mathbf{u}$	velocity vector
$V_{\max}$	maximum velocity
W	Kernel function
$\dot{\gamma}$	shear rate
Δt	time step
$\Delta\mathbf{u}$	changed velocity
η	small number to avoid singularity
μ	constant viscosity of water
$\mu_0(\mu_\infty)$	viscosity at very low (high) shear
μ_B	Bingham viscosity
μ_{eff}	effective viscosity
ρ	fluid density
ρ_0	initial density
τ_B	Bingham yield stress
∇	gradient operator
∇^2	Laplacian operator
$\sum$	summation operator

REFERENCES

1. Wiegel R. Laboratory studies of gravity waves generated by the movement of a submarine body. *Transactions—American Geophysical Union* 1955; **36**(5):759–774.
2. Iwasaki S. Experimental study of a Tsunami generated by a horizontal motion of a sloping bottom. *Bulletin of the Earthquake Research Institute* 1982; **57**:239–262.
3. Heinrich P. Nonlinear water waves generated by submarine and aerial landslides. *Journal of Waterways, Port, Coastal, and Ocean Engineering* 1992; **118**(3):249–266.
4. Watts P. Wave maker curves for Tsunamis generated by underwater landslides. *Journal of Waterways, Port, Coastal, and Ocean Engineering* 1998; **124**(3):127–137.
5. Fritz HM, Hager WH, Minor HE. Near field characteristics of landslide generated impulse waves. *Journal of Waterway, Port, Coastal, and Ocean Engineering* 2004; **130**(6):287–302.
6. Jiang L, LebLond PH. The coupling of a submarine slide and the surface waves which it generates. *Journal of Geophysical Research* 1992; **97**(C8, 12):731–744.
7. Rzadkiewicz S, Mariotti C, Heinrich P. Numerical simulation of submarine landslides and their hydraulic effects. *Journal of Waterway, Port, Coastal, and Ocean Engineering* 1997; **123**(4):149–157.
8. Grilli ST, Watts P. Modeling of waves generated by a movingsubmerged body. Applications to underwater landslides. *Journal of Engineering Analysis with Boundary Elements* 1999; **23**:645–656.
9. Ataie-Ashtiani B, Najafi-Jilani A. Prediction of submerged landslide generated waves in dam reservoirs: an applied approach. *Dam Engineering* 2006; **XVII**(3):135–155.
10. Ataie-Ashtiani B, Najafi-Jilani A. Higher-order Boussinesq-type model with moving bottom boundary: applications to submarine landslide Tsunami waves. *International Journal for Numerical Methods in Fluids* 2007; **53**(6): 1019–1048.
11. Ataie-Ashtiani B, Malek Mohammadi S. Near-field amplitude of subaerial landslide generated waves in dam reservoirs. *Dam Engineering* 2007; **XVII**(4):197–222.
12. Ataie-Ashtiani B, Farhadi L. A stable moving-particle semi-implicit method for free surface flows. *Fluid Dynamic Research* 2006; **38**(4):241–256.
13. Koshizuka S, Oka Y. Moving-particle semi-implicit method for fragmentation of incompressible fluid. *Journal of Nuclear Science and Engineering* 1996; **123**:421–434.

DOI: 10.1002/fld

14. Shao SD, Gotho H. Turbulance particle models for tracking free surfaces. *Journal of Hydraulic Research* 2005; **43**(3):276–289.
15. Koshizuka S, Ikeda H, Oka Y. Numerical analysis of fragmentation mechanisms in vapor explosion. *Nuclear Engineering and Design* 1999; **189**:423–433.
16. Gotoh H, Sakai T. Lagrangian simulation of breaking waves using particle method. *Coastal Engineering Journal* 1999; **41**(3–4):303–326.
17. Gotoh H, Sakai T, Hayashi M. Lagrangian two-phase flow model for the wave generation process due to large-scale landslides. *Asian and Pacific Coastal Engineering* 2001; **October 18–21**:176–185.
18. Lucy L. A numerical approach to the testing of fusion process. *Astronomical Journal* 1977; **82**:1013–1024.
19. Monaghan JJ. Simulating free surface flows with SPH. *Journal of Computational Physics* 1994; **110**:399–406.
20. Lo EYM, Shao S. Simulation of near-shore solitary wave mechanics by an incompressible SPH method. *Journal of Applied Ocean Research* 2002; **24**:275–286.
21. Shao SD, Lo EYM. Incompressible SPH method for simulating Newtonian and non-Newtonian flows with a free surface. *Advances in Water Resources* 2003; **26**(7):787–800.
22. Monaghan JJ, Cas RF, Kos A, Hallworth M. Gravity currents descending a ramp in a stratified tank. *Journal of Fluid Mechanics* 1999; **379**:39–70.
23. Gómez-Gesteira M, Dalrymple RA. Using a three-dimensional smoothed particle hydrodynamics method for wave impact on a tall structure. *Journal of Waterway*, *Port*, *Coastal*, *and Ocean Engineering* (ASCE) 2004; **130**(2).
24. Dalrymple RA, Knio O, Cox DT, Gesteira M, Zou S. Using a Lagrangian particle method for deck overtopping. *Proceedings of Waves 2001*, Reston, VA, ASCE, 2002; 1082–1091.
25. Issa R, Lee ES, Violeau D, Laurence D. Incompressible separated flows simulations with the smoothed particle hydrodynamics gridless method. *International Journal for Numerical Methods in Fluids* 2004; **47**(10–11): 1101–1106.
26. De Girolamo P, Wu TR, Liu PLF, Panizzo A, Bellotti G, Di Risio M. Numerical simulation of three dimensional Tsunamis water waves generated by landslides: comparison between physical model results, VOF, SPH and depth-integrated models. *ICCE Conference*, San Diego, 2006.
27. Panizzo A, Dalrymple RA. SPH modelling of underwater landslide generated waves. *ICCE 2004 Conference*, Lisbon, 2004.
28. Panizzo A, Cuomo G, Dalrymple RA. 3D-SPH simulation of landslide generated waves. *ICCE 2006 Conference*, San Diego, 2006.
29. Gallati M, Braschi G. SPH simulation of the wave produced by a block falling into a water tank. *Proceedings of International Conference on Fluid Flow Technologies* (*CMFF'03*), Budapest, 2003.
30. Gallati M, Braschi G, Falappi S. SPH simulations of the waves produced by a block falling into a reservoir. *Il Nuovo Cimento* 2005; **28C**(2):129–140.
31. Monaghan JJ, Kos A, Issa N. Fluid motion generated by impact. *Journal of Waterway*, *Port*, *Coastal*, *and Ocean Engineering* 2003; **129**(6):250–259.
32. Monaghan JJ. Smoothed particle hydrodynamics. *Annual Review of Astronomy and Astrophysics* 1992; **130**: 543–574.
33. Shobeyri G. Modifying and using incompressible smoothed particle hydrodynamics to simulate waves due to landslides. *M.Sc. Thesis*, Department of Civil Engineering, Sharif University of Technology, 2006.
34. Monaghan JJ, Kos A. Scott Russell's wave generator. *Physics of Fluids* 2000; **12**:622–630.
35. Barnes HA, Hutton JF, Walters K. *An Introduction to Rheology*. Elsevier: Amsterdam, 1989.

DOI: 10.1002/fld